

# Real-time Estimation of Bound Water Concentration during Lyophilization with Temperature-based State Observers

Prakitr Srisuma<sup>1,2,3</sup>, George Barbastathis<sup>1,3</sup>, and Richard D. Braatz<sup>1,2\*</sup>

<sup>1</sup>*Center for Computational Science and Engineering, Massachusetts Institute of Technology, Cambridge, MA 02139, USA*

<sup>2</sup>*Department of Chemical Engineering, Massachusetts Institute of Technology, Cambridge, MA 02139, USA*

<sup>3</sup>*Department of Mechanical Engineering, Massachusetts Institute of Technology, Cambridge, MA 02139, USA*

---

## Abstract

Lyophilization (aka freeze drying) has been shown to provide long-term stability for many crucial biotherapeutics, e.g., mRNA vaccines for COVID-19, allowing for higher storage temperature. The final stage of lyophilization, namely secondary drying, entails bound water removal via desorption, in which accurate prediction of bound water concentration is vital to ensuring the quality of the lyophilized product. This article proposes a novel technique for real-time estimation of the residual moisture during secondary drying in lyophilization. A state observer is employed, which combines temperature measurement and mechanistic understanding of heat transfer and desorption kinetics, without requiring any online concentration measurement. Results from both simulations and experimental data show that the observer can accurately estimate the concentration of bound water in real time for all possible concentration levels, operating conditions, and measurement noise. This framework can also be applied for monitoring and control of the residual moisture in other desorption-related processes.

**Keywords**— Lyophilization, Freeze drying, Secondary drying, Bound water, Desorption, State observer

---

## 1 Introduction

Lyophilization, also known as freeze drying, is a process used to increase the stability of biotherapeutics in pharmaceutical manufacturing [1]. In recent studies, lyophilization has been shown to provide long-term stability for mRNA vaccines, allowing these vaccines to be stored at higher temperature while preserving their functionality [2, 3]. This promising advancement could play an important role in future mRNA-based therapeutic manufacturing, in particular vaccine distribution in regions where a cold supply chain is lacking.

Three stages of lyophilization comprise (1) freezing, (2) primary drying, and (3) secondary drying, respectively. In freezing, the product and liquid solvent (usually water) are frozen, in which the free water becomes ice crystals, whereas water bound to the organic material between the crystals (aka bound water) retains its noncrystalline state [4]. Primary drying entails the sublimation of the ice crystals [5]. Subsequently, secondary drying is conducted at higher temperature to remove the bound water via desorption [6, 7]. The stability of a lyophilized product is significantly influenced by the amount of bound water, and so monitoring the concentration of bound water is most important [4]. One of the most common techniques is the Karl Fischer titration, which requires sampling of the vial for offline measurements [4, 8, 9]. To avoid process interruption, some online or non-invasive techniques

---

\*Corresponding author. Email: braatz@mit.edu

such as near-infrared (NIR) spectroscopy [10] and tunable diode laser absorption spectroscopy (TDLAS) [11] have been proposed. Detailed discussion of tools for the monitoring of secondary drying can be found in Ref. [4].

Instead of direct measurement, a state observer (aka state estimator, observer, estimator) can be used to estimate states that are not measured [12]; the process is known as state estimation. A well-designed observer can replace expensive and complicated sensors in the system, reducing the total cost and complexity of operation. The principle of state estimation is to combine available measurement data of some states with the physics of a system represented by a mechanistic model, and use that information to estimate the other states that are not measured. A variety of mechanistic models for lyophilization are available [1, 6, 9, 13–18], which establishes a solid foundation for constructing a reliable observer.

Various state observers have been proposed and successfully implemented in chemical processes [19]. In the context of lyophilization, state observers have been extensively studied and applied to the primary drying step, which aims at estimating the temperature, interface position (amount of ice), and relevant parameters such as the heat transfer coefficient [20–27]. Besides monitoring, some other applications such as process optimization [28] and control [29, 30] have been demonstrated. Observer design for primary drying is straightforward as it mainly concerns heat transfer associated with sublimation and, in many cases, an observer is not even needed as heat transfer-related quantities, e.g., temperature, can be measured easily. In secondary drying, heat transfer and desorption dynamics are coupled, making the observer design more challenging and valuable. Currently, applications of state estimation to secondary drying are very limited. The only literature that proposed a state estimation-like strategy for secondary drying is Ref. [9]; the technique is referred to as a soft sensor which requires measurement of the desorption flux for estimating the residual moisture. The procedure in Ref. [9] does not exploit the mathematical structure of a state observer; the key idea is to iteratively solve the optimization to find the moisture content that matches the measured desorption rate. This technique also requires additional equipment specifically for measuring the desorption flux.

In this article, a new technique is proposed for real-time estimation of bound water concentration during desorption, and is applied to secondary drying in lyophilization. The technique relies on a state observer that estimates the concentration of bound water by using temperature measurement and mechanistic understanding of heat transfer and desorption kinetics. The proposed observer is extensively tested with various simulations and experiments. Since accurate bound water measurement is not trivial and involves complex equipment and procedures [31], our observer is formulated such that the only input required is temperature measurement, which is straightforward and very common in every step of lyophilization [4, 32], allowing for the simplest setup and operation compared to any other methods. The proposed framework can also be easily and systematically extended to other desorption-related processes.

## 2 Mechanistic Modeling

A mechanistic model is an important element in a state observer as it contains the knowledge about the physics of a system. Our model is formulated in the rectangular coordinate system by considering one spatial dimension ( $z$ ) and time ( $t$ ) as pictorially shown in Fig. 1. For lyophilization, 1D modeling is nearly always used because its accuracy is comparable to that of multidimensional modeling while being much computationally cheaper and less complicated, whereas 0D modeling (lumped capacity) is not sufficiently accurate [33].

In secondary drying, there are three important transport phenomena, namely (1) heat transfer within the dried product, (2) desorption of the water vapor from the surface of the dried product, and (3) mass transfer of the water vapor in the pores of the dried product [1, 6, 13–16].

The first part of the model describes the heat transfer. The energy balance of the dried product is

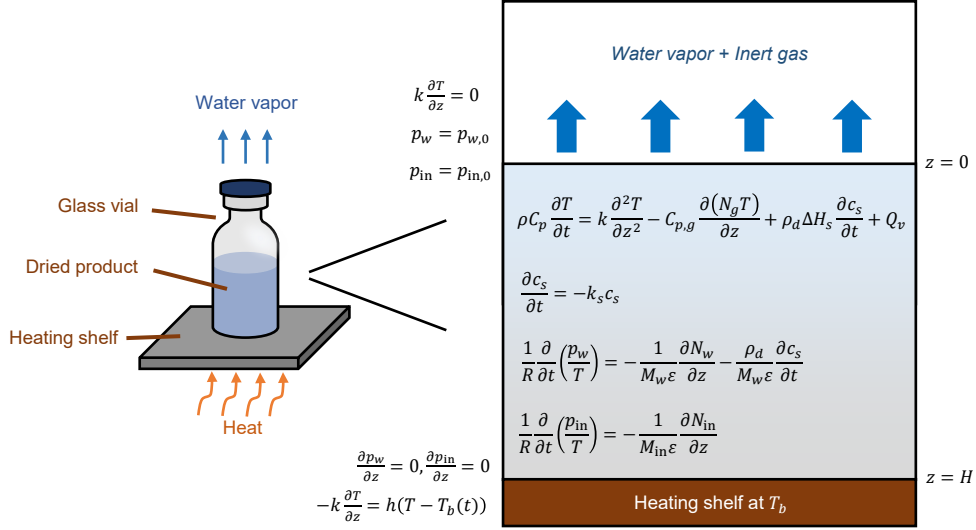


**Figure 1:** Schematic diagram showing a mechanistic model for the secondary drying step in lyophilization.

given by [1, 13–17]

$$\rho C_p \frac{\partial T}{\partial t} = k \frac{\partial^2 T}{\partial z^2} - C_{p,g} \frac{\partial(N_g T)}{\partial z} + \rho_d \Delta H_s \frac{\partial c_s}{\partial t} + Q_v, \quad t > 0, \quad (1)$$

where  $T(z, t)$  is the product temperature,  $c_s(z, t)$  is the bound water concentration (aka moisture content, residual water),  $\Delta H_s$  is the enthalpy of desorption,  $\rho$  is the effective density,  $\rho_d$  is the density of the dried product,  $k$  is the effective thermal conductivity,  $C_p$  is the effective heat capacity,  $H$  is the height of the dried product,  $N_g$  is the total mass flux of the gas (water vapor and inert gas), and  $C_{p,g}$  is the heat capacity of the gas. Here effective parameters consider the properties of both solid and gas in the pores, the subscript  $d$  denotes parameters for the dried product only (solid and vacuum), the subscript  $g$  denotes parameters for the gas phase only, and the subscript  $s$  denotes parameters related to desorption.

The additional term  $Q_v$  in (1) describes the effect of microwave irradiation, which provides volumetric heating to the product [34, 35]. This study focuses on conventional lyophilization, i.e., no microwave, and so this term is set to 0 by default. Nevertheless, it is worth noting that our model and observer are designed to accommodate microwave lyophilization as well (see Supplementary Information). The physics of microwave heating is related to dielectric heating, which is influenced by the electric field strength, the microwave frequency, and the dielectric loss factor of each material; detailed discussion can be found in [17, 35, 36]. Nevertheless, this information is not always readily available for all systems, so we model the microwave heating as a single composite term  $Q_v$  in this case.

The bottom surface of the dried product is heated by the heating shelf, following Newton’s law of cooling,

$$-k \frac{\partial T}{\partial z}(H, t) = h(T(H, t) - T_b(t)), \quad t > 0, \quad (2)$$

where  $h$  is the heat transfer coefficient at the bottom and  $T_b(t)$  is the bottom shelf temperature. Typically the shelf temperature initially increases linearly as a function of time,

$$T_b(t) = rt + T_{b,0}, \quad (3)$$

where  $T_{b,0}$  is the initial shelf temperature and  $r$  is the temperature ramp-up rate. After reaching the maximum temperature  $T_{b,\max}$ , the shelf temperature is kept constant at that value.\* At the top surface, heat transfer is negligible compared to the bottom surface, and thus the boundary condition is

$$k \frac{\partial T}{\partial z}(0, t) = 0, \quad t > 0. \quad (4)$$

\*The methods apply for general  $T_b(t)$ .

The initial temperature of the frozen region is spatially uniform at  $T_0$ ,

$$T(x, 0) = T_0, \quad 0 \leq z \leq H. \quad (5)$$

As secondary drying takes place after primary drying,  $T_0$  can be set to the sublimation temperature.

The second part of the model concerns bound water desorption. It has been widely accepted in the literature that the linear driving force model can accurately predict the dynamics of bound water desorption despite being one of the simplest adsorption/desorption models [1, 6, 9, 13, 15, 16, 18, 37]. Hence, the desorption kinetics of bound water is described by

$$\frac{\partial c_s}{\partial t} = -k_s c_s, \quad (6)$$

where  $k_s$  is the rate constant for desorption that exhibits Arrhenius temperature dependence [1, 15, 18]

$$k_s = A e^{-E_a/RT}, \quad (7)$$

where  $A$  is the frequency factor (aka collision frequency) and  $E_a$  is the activation energy. This representation is identical to the first-order kinetics for chemical reactions. It has been shown via both experiment and simulation that bound water desorption is negligible during primary drying [15, 16], so the initial concentration of bound water in secondary drying is assumed to be uniform at  $c_{s,0}$ ,

$$c_s(z, 0) = c_{s,0}, \quad 0 \leq z \leq H. \quad (8)$$

The last part of the model focuses on mass transfer of gas/vapor in the pores of the dried product, which usually consists of water vapor ( $w$ ) and inert gas ( $in$ ). The continuity equations, assuming ideal gas behaviors for both components, are [1, 6, 13–17]

$$\frac{1}{R} \frac{\partial}{\partial t} \left( \frac{p_w}{T} \right) = -\frac{1}{M_w \varepsilon} \frac{\partial N_w}{\partial z} - \frac{\rho_d}{M_w \varepsilon} \frac{\partial c_s}{\partial t}, \quad (9)$$

$$\frac{1}{R} \frac{\partial}{\partial t} \left( \frac{p_{in}}{T} \right) = -\frac{1}{M_{in} \varepsilon} \frac{\partial N_{in}}{\partial z}, \quad (10)$$

where  $p(z, t)$  is the partial pressure,  $N(z, t)$  is the mass flux (mass flow rate per cross sectional area),  $M$  is the molar mass,  $R$  is the gas constant,  $\varepsilon$  is the porosity, and the subscripts  $w$  and ‘in’ denote the water vapor and inert gas, respectively. The expression for  $N$  is usually modeled by the dusty-gas model [6, 13–16]. Note that the total mass flux  $N_g$  in (1) is  $N_w + N_{in}$ . The initial conditions for both components are

$$p_w(z, 0) = p_{w,0}, \quad 0 \leq z \leq H, \quad (11)$$

$$p_{in}(z, 0) = p_{in,0}, \quad 0 \leq z \leq H, \quad (12)$$

where  $p_{w,0}$  and  $p_{in}$  are usually defined by the condenser located downstream of the lyophilizer. The boundary conditions are

$$p_w(0, t) = p_{w,0}, \quad t > 0, \quad (13)$$

$$p_{in}(0, t) = p_{in,0}, \quad t > 0, \quad (14)$$

$$\frac{\partial p_w}{\partial x}(H, t) = 0, \quad t > 0, \quad (15)$$

$$\frac{\partial p_{in}}{\partial x}(H, t) = 0, \quad t > 0. \quad (16)$$

The main objective of secondary drying is to remove bound water; hence, the concentration of bound water  $c_s$  is usually the variable of interest [4, 9, 15, 18]. As can be observed from the model equations, the

desorption kinetics are mainly influenced by the temperature  $T$ , so the concentration of bound water can be predicted accurately with only the energy balance and desorption kinetics equations [18, 33, 38]. As such, without loss of generality, mass transfer equations are omitted from the simulations and observer design. This approach simplifies the model equations, parameter estimation, and observer/control design; this simplification does not significantly affect the accuracy of the process model and state observer (see the results in Section 4.1). Nevertheless, it is important to note that mass transfer equations provide information about pressure, so it could be useful for applications related to pressure control and optimization, which is not the scope of this work.

In this work, the above mechanistic model is simulated numerically. The model equations are spatially discretized using the finite volume method, with the details given in Supplementary Information. The final discretized equations can be written as

$$\frac{d\mathbf{x}}{dt} = \mathbf{F}(\mathbf{x}) + \mathbf{B}\mathbf{u}, \quad (17)$$

with the state  $\mathbf{x}$  and manipulated variable  $\mathbf{u}$  defined as

$$\mathbf{x} = \begin{bmatrix} \mathbf{T} \\ \mathbf{c}_s \end{bmatrix}, \quad (18)$$

$$\mathbf{u} = \begin{bmatrix} T_b \\ Q_v \end{bmatrix}, \quad (19)$$

where  $\mathbf{T} \in \mathbb{R}^m$  collects the product temperatures  $T_1, \dots, T_m$ ,  $\mathbf{c}_s \in \mathbb{R}^m$  collects the bound water concentrations  $(c_{s,1}, \dots, c_{s,m})$ ,  $m$  is the number of grid points in the spatial domain,  $\mathbf{F} \in \mathbb{R}^{2m}$  is a nonlinear vector function, and  $\mathbf{B} \in \mathbb{R}^{2m \times 2}$  is a matrix. To facilitate the observer design, (17) can be rewritten as

$$\frac{d\mathbf{T}}{dt} = \mathbf{F}_T(\mathbf{T}, \mathbf{c}_s) + \mathbf{B}_T\mathbf{u}, \quad (20)$$

$$\frac{d\mathbf{c}_s}{dt} = \mathbf{F}_c(\mathbf{T}, \mathbf{c}_s) + \mathbf{B}_c\mathbf{u}, \quad (21)$$

where  $\mathbf{F}_T \in \mathbb{R}^m$ ,  $\mathbf{B}_T \in \mathbb{R}^{m \times 2}$  represent the dynamics of the temperature part and  $\mathbf{F}_c \in \mathbb{R}^m$  is the nonlinear function for the concentration part. The finite volume method transforms the original partial differential equations (PDEs) into a system of ordinary differential equations (ODEs). The final ODEs (20) and (21) can be integrated by commercial ODE solvers, in which `ode15s` in MATLAB is used in this work. This technique is known as the method of lines [39].

Lastly, define the average temperature and average concentration,

$$T_{\text{avg}} = \frac{1}{m} \sum_{i=1}^m T_i, \quad (22)$$

$$c_{s,\text{avg}} = \frac{1}{m} \sum_{i=1}^m c_{s,i}. \quad (23)$$

### 3 State Observer

A state observer (aka state estimator, observer, estimator) is a tool in control theory used for reconstructing the unmeasured states given the available measurements and mechanistic understanding of a system; the process is referred to as state estimation. Those unmeasured states could be internal states that cannot be measured or states that are difficult to measure. Measuring the temperature during lyophilization is relatively simple and accurate, so we design a state observer that uses the temperature measurement to estimate the concentration of bound water, the most important process variable in secondary drying.

State estimation is critical for process monitoring and control, in which the information of the unmeasured states is needed. Various state observers have been proposed and employed [19]. The Luenberger observer [12] has a simple mathematical structure and is computationally efficient for both linear and nonlinear processes, which has resulted in its widespread use in various applications [40].

### 3.1 Mathematical structure of a state observer

Applying the Luenberger observer to the final model equation (17) results in

$$\frac{d\hat{\mathbf{x}}}{dt} = \mathbf{F}(\hat{\mathbf{x}}) + \mathbf{B}\mathbf{u} + \mathbf{L}(\hat{\mathbf{y}} - \mathbf{y}), \quad (24)$$

where  $\hat{\mathbf{x}} \in \mathbb{R}^{2m}$  is the estimated state predicted by the observer,  $\mathbf{y}$  is the measured outputs,  $\hat{\mathbf{y}}$  is the estimated outputs, and  $\mathbf{L}$  is the observer gain. Similar to the actual state defined by (18), the estimated state  $\mathbf{x}$  is

$$\hat{\mathbf{x}} = \begin{bmatrix} \hat{\mathbf{T}} \\ \hat{\mathbf{c}}_s \end{bmatrix}. \quad (25)$$

where  $\hat{\mathbf{T}} \in \mathbb{R}^m$  is the estimated temperature and  $\hat{\mathbf{c}}_s \in \mathbb{R}^m$  is the estimated concentration. The measured output is the temperature profile of the product, so

$$\mathbf{y} = \mathbf{T} + \mathbf{n}, \quad (26)$$

$$\hat{\mathbf{y}} = \hat{\mathbf{T}}, \quad (27)$$

where  $\mathbf{n} \in \mathbb{R}^m$  is the sensor noise. The most important part of the observer is the observer gain  $\mathbf{L} \in \mathbb{R}^{2m \times m}$ , which directly affects the performance of the observer. Depending on the knowledge of the system, different strategies can be used to design the observer gain.

To simplify the observer design, we separate the observer gain matrix  $\mathbf{L}$  into two parts corresponding to the temperature and concentration, that is,

$$\mathbf{L} = \begin{bmatrix} \mathbf{L}_T \\ \mathbf{L}_c \end{bmatrix}, \quad (28)$$

where  $\mathbf{L}_T \in \mathbb{R}^{m \times m}$  is the observer gain for the temperature part and  $\mathbf{L}_c \in \mathbb{R}^{m \times m}$  is the observer gain for the concentration part. Consequently, (24) can be rewritten as

$$\frac{d\hat{\mathbf{T}}}{dt} = \mathbf{F}_T(\hat{\mathbf{T}}, \hat{\mathbf{c}}_s) + \mathbf{B}_T\mathbf{u} + \mathbf{L}_T(\hat{\mathbf{T}} - \mathbf{T}), \quad (29)$$

$$\frac{d\hat{\mathbf{c}}_s}{dt} = \mathbf{F}_c(\hat{\mathbf{T}}, \hat{\mathbf{c}}_s) + \mathbf{B}_c\mathbf{u} + \mathbf{L}_c(\hat{\mathbf{T}} - \mathbf{T}). \quad (30)$$

Here the first part of the observer (29) estimates the product temperature, while the second part (30) estimates the residual moisture. Separating the observer gains allows each part of the observer to be designed separately while still respecting the coupling of the states in the original model.

The final step is to design the observer gains  $\mathbf{L}_T$  and  $\mathbf{L}_c$ . The current observer gains  $\mathbf{L}_T$  and  $\mathbf{L}_c$  are  $m \times m$  matrices, which leaves many degrees of freedom in the observer design. Therefore, we parameterize the observer gain matrices by

$$\mathbf{L}_T = L_T \mathbf{J}_m, \quad (31)$$

$$\mathbf{L}_c = L_c \mathbf{J}_m, \quad (32)$$

where  $L_T, L_c$  are the real scalars and  $\mathbf{J}_m$  is an  $m \times m$  matrix of ones. This parameterization suggests that the temperature measurement at each location contributes equally to the observer, leaving only

two degrees of freedom for the design, which are the values of  $L_T$  and  $L_c$ . A well-designed observer should converge the estimated states converge to the true states fast compared to the time scale of the process. The convergence can be evaluated via the estimation errors defined as

$$\mathbf{e}_T = |\hat{\mathbf{T}} - \mathbf{T}|, \quad (33)$$

$$\mathbf{e}_c = |\hat{\mathbf{c}}_s - \mathbf{c}_s|, \quad (34)$$

where  $\mathbf{e}_T$  is the estimation error for temperature and  $\mathbf{e}_c$  is the estimation error for concentration. A zero estimation error indicates the convergence of the estimated state.

### 3.2 Modified state observer

The state observer proposed in Section 3.1 receives spatially distributed temperature measurement  $\mathbf{T}$  and provides estimates of both temperature  $\hat{\mathbf{T}}$  and concentration  $\hat{\mathbf{c}}_s$  in real time. Although having a spatially distributed temperature measurement is feasible using current thermal imaging sensors, traditional lyophilization systems do not have such sensors. For example, a thermocouple used for temperature measurement is usually in contact with the bottom of the product, and so only the bottom temperature is available [4, 6]. Therefore, we propose an alternative state observer for this scenario.

For convenience, we denote this alternative as a *modified state observer*. Modifying the original observer to take the bottom temperature measurement instead of the spatial temperature measurement results in the output vectors  $\mathbf{y}$  and  $\hat{\mathbf{y}}$

$$\mathbf{y} = T_p + \mathbf{n}, \quad (35)$$

$$\hat{\mathbf{y}} = \hat{T}_p, \quad (36)$$

where the measurement noise  $\mathbf{n}$  is a real scalar and  $T_p$  is the bottom temperature. In the state vector,  $T_p$  corresponds to the last element of  $\mathbf{T}$ . As a result, the equations for this observer are

$$\frac{d\hat{\mathbf{T}}}{dt} = \mathbf{F}_T(\hat{\mathbf{T}}, \hat{\mathbf{c}}_s) + \mathbf{B}_T \mathbf{u} + \mathbf{L}_T(\hat{T}_p - T_p), \quad (37)$$

$$\frac{d\hat{\mathbf{c}}_s}{dt} = \mathbf{F}_c(\hat{\mathbf{T}}, \hat{\mathbf{c}}_s) + \mathbf{B}_c \mathbf{u} + \mathbf{L}_c(\hat{T}_p - T_p), \quad (38)$$

where  $\mathbf{L}_T \in \mathbb{R}^m$  and  $\mathbf{L}_c \in \mathbb{R}^m$  are the observer gains. Similarly, we can parameterize  $\mathbf{L}_T$  and  $\mathbf{L}_c$  using the vector of ones (instead of the matrix of ones as used for the original state observer) such that the only design parameters are the real scalars  $L_T$  and  $L_c$ . It is worth noting that, since the observer structure and equations are different, the values of  $L_T$  and  $L_c$  used for the state observer and modified observers are also different, as shown in the Implementation to Real Systems section.

Most of the results in this article are based on the original state observer as it uses the most complete measurement information, with some results and discussion on the modified observer in the Implementation to Real Systems section.

### 3.3 Observer design strategies

The structure of the state observer for estimating the concentration of bound water is illustrated in Fig. 2. The proposed observer has the physics of heat transfer and bound water desorption embedded in  $\mathbf{F}_T$  and  $\mathbf{F}_c$ , which is given by the mechanistic model. The temperature measurement is fed to the observer terms represented by the observer gains  $\mathbf{L}_T$  and  $\mathbf{L}_c$ . The observer combines the information from the mechanistic model and temperature measurement to converge the estimated bound water concentration to the true values without the need for concentration measurement.



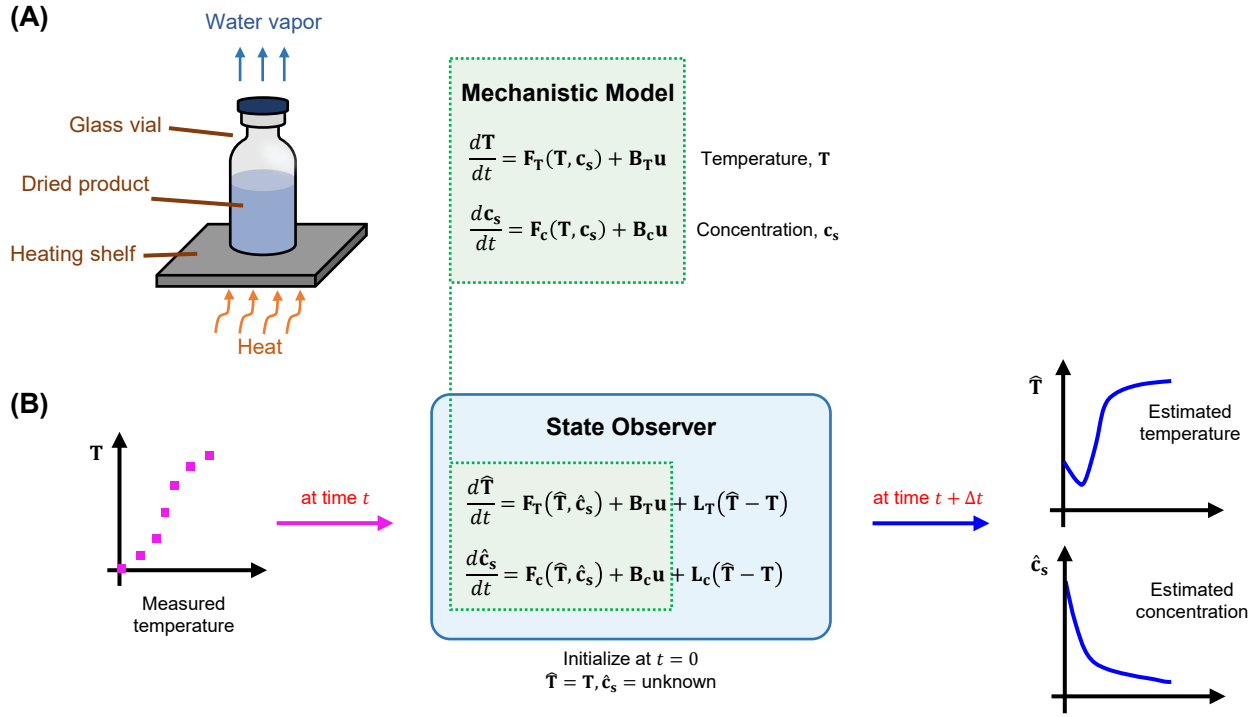


**Figure 2:** (A) Schematic diagram of the typical lyophilization process. In secondary drying, a glass vial which contains the dried product is heated such that the bound water is desorbed and removed from the product at the top. The mechanistic model is used to describe heat transfer and desorption dynamics. (B) Structure of the proposed state observer. The observer receives the measured temperature and the control input (i.e., the shelf temperature and microwave power) at time step  $t$ , and estimates the temperature and concentration at the next time step. To initialize the observer at  $t = 0$ , the estimated temperature can be set to the measured value. The initial concentration is completely unknown due to no measurement, so it can be set to some realistic values obtained from the literature or previous experiment.

The most important consideration for observer design is to ensure that the estimated states converge to the true states fast compared to the time scale of the process; i.e., the estimation error converges to zero. In addition, the observer should be designed to be insensitive to measurement noise, that is, that the estimated states are not significantly polluted by measurement noise. The observer gains  $L_T$  and  $L_c$  play an important role in the overall performance of the observer. Thus, observer design entails selection of the values of these gains. Instead of attempting to search over all elements of the full observer gain matrices  $L_T$  and  $L_c$ , we show in Sections 3.1 and 3.2 that  $L_T$  and  $L_c$  be parameterized and rewritten as a product of the real scalar  $L_T$  or  $L_c$  and the matrix of ones, so the only design parameters are the real scalars  $L_T$  and  $L_c$ .

The design procedure for the observer gains  $L_T$  and  $L_c$  consists of two main steps. The first step relies entirely on the mechanistic model and simulation, where the model prediction represents the true state of the system. In this step, a series of simulations are run with different observer gains and parameters to investigate the dynamics of the system and observer under various conditions, and then the observer gains are selected based on the overall performance of the observer. The second step takes the real data/measurement from experiment into account, and so the observer gains are fine-tuned to be specific to the real system. These two steps are denoted as *simulation-based observer design* and *experiment-based observer design*. The former allows for different operating conditions and noise profiles to be tested so that the resulting design can cover many possible scenarios, whereas the latter is primarily specific to the system where the real data are available. The benefit of this two-step procedure is that it allows the observer to be designed efficiently without any complicated mathematical analysis, and hence this technique is practical and has been used in industrial applications. For the system,  $L_T$  and  $L_c$  have the units of  $s^{-1}$  and  $\text{kg water}/(\text{kg solid} \cdot \text{K} \cdot \text{s})$ , but only the magnitudes of  $L_T$  and  $L_c$  are reported to keep the plots simple and easy to visualize.

This two-step procedure is simple and practical as it requires only simulations and experimental data, without any detailed mathematical analysis. This technique is generally sufficient for observer design in



many applications. In addition to this technique, a more systematic way of simulation-based observer design is to analyze the mathematical structure of the observer, in which more useful insights into the observer dynamics can be extracted. To begin this analysis, we first define the Jacobian of the nonlinear function  $\mathbf{F}$  in (17) as

$$\mathbf{F}' = \frac{\partial \mathbf{F}}{\partial \mathbf{x}}, \quad (39)$$

where  $\mathbf{F}'$  can be calculated analytically or numerically. One of the simplest but efficient ways of analyzing a nonlinear state observer is to approximate the nonlinear parts with the linear equations, i.e., linearization. Linearization of the model equation (17) results in

$$\frac{d\mathbf{x}}{dt} = \mathbf{F}_{\text{ref}} + \mathbf{F}'_{\text{ref}}(\mathbf{x} - \mathbf{x}_{\text{ref}}) + \mathbf{B}\mathbf{u}, \quad (40)$$

where  $\mathbf{F}_{\text{ref}} = \mathbf{F}(\mathbf{x}_{\text{ref}})$  is the function  $\mathbf{F}$  evaluated at  $\mathbf{x}_{\text{ref}}$ ,  $\mathbf{F}'_{\text{ref}} = \mathbf{F}'(\mathbf{x}_{\text{ref}})$  is the Jacobian  $\mathbf{F}'$  evaluated at  $\mathbf{x}_{\text{ref}}$ , and  $\mathbf{x}_{\text{ref}}$  is the reference state. The average temperature and concentration are used as the reference state, which is constant and uniform. Note that, although there is no real-time concentration measurement available, the average concentration used in this analysis can be obtained via offline measurement during the design and development phase as discussed in the Results section. Alternatively, the literature value could be used, but that would result in a less accurate analysis. With (40), the linearized state observer is

$$\frac{d\hat{\mathbf{x}}}{dt} = \mathbf{F}_{\text{ref}} + \mathbf{F}'_{\text{ref}}(\hat{\mathbf{x}} - \mathbf{x}_{\text{ref}}) + \mathbf{L}(\hat{\mathbf{y}} - \mathbf{y}) + \mathbf{B}\mathbf{u}. \quad (41)$$

Subtracting (40) from (41) yields

$$\frac{d}{dt}(\hat{\mathbf{x}} - \mathbf{x}) = \mathbf{F}'_{\text{ref}}(\hat{\mathbf{x}} - \mathbf{x}) + \mathbf{L}(\hat{\mathbf{y}} - \mathbf{y}), \quad (42)$$

In this case, it is useful to write  $\mathbf{y}$  and  $\hat{\mathbf{y}}$  as a function of  $\mathbf{x}$ , that is,

$$\mathbf{y} = \mathbf{C}\mathbf{x} + \mathbf{n}, \quad (43)$$

$$\hat{\mathbf{y}} = \mathbf{C}\hat{\mathbf{x}}, \quad (44)$$

where

$$\mathbf{C} = [\mathbf{I}_m \quad \mathbf{0}_{m,m}], \quad (45)$$

where  $\mathbf{I}_m$  is an  $m \times m$  identity matrix and  $\mathbf{0}_{m,m}$  is an  $m \times m$  zero matrix. With this definition, it is easy to see that (43) and (44) are identical to (26) and (27). Substituting (43) and (44) into (41) followed by rearranging gives that

$$\frac{d}{dt}(\hat{\mathbf{x}} - \mathbf{x}) = (\mathbf{F}'_{\text{ref}} + \mathbf{L}\mathbf{C})(\hat{\mathbf{x}} - \mathbf{x}) - \mathbf{L}\mathbf{n}, \quad (46)$$

which is a linear ODE that gives the criterion for observer design, where the eigenvalues of the matrix  $\mathbf{F}'_{\text{ref}} + \mathbf{L}\mathbf{C}$  characterize the dynamics of the observer. For the estimation error  $\hat{\mathbf{x}} - \mathbf{x}$  to converge to zero, the observer gains  $L_T$  and  $L_c$  must be chosen such that the real parts of all eigenvalues of the matrix  $\mathbf{F}'_{\text{ref}} + \mathbf{L}\mathbf{C}$  are negative. Besides, the estimation error should decay significantly faster the time scale of the process, i.e., the eigenvalues of the original matrix  $\mathbf{F}'_{\text{ref}}$ . Oscillation should also be minimized, which is governed by the imaginary parts of all eigenvalues. This approach allows the systematic selection of the values of  $L_T$  and  $L_c$  to specify the dynamics of the observer.

An important parameter of interest that can be extracted from the above analysis is a time constant, denoted as  $\tau$ , which describes how fast the estimation error reduces to zero. Before discussing the time constant, denote the eigenvalues of the matrix  $\mathbf{F}'_{\text{ref}} + \mathbf{L}\mathbf{C}$  from the largest to the smallest as  $\lambda_1, \lambda_2, \dots, \lambda_{2m}$ , in which  $\lambda_1$  is the largest and  $\lambda_{2m}$  is the smallest. As  $\mathbf{F}'_{\text{ref}} + \mathbf{L}\mathbf{C}$  is a  $2m \times 2m$  matrix, there are  $2m$  eigenvalues in total. The simplest choice for approximating the time constant is to consider the slowest eigenvalue:

$$\tau = \frac{1}{|\text{Re}(\lambda_{2m})|}. \quad (47)$$

In this particular application, a much more accurate approximation is

$$\tau = \frac{1}{|\operatorname{Re}(\lambda_{m+1})|}, \quad (48)$$

which is justified in Supplementary Information by a detailed mathematical analysis on the effects of all eigenvalues. The approximation (48) is sufficiently accurate for all parameter values for the mechanistic model, numerical methods, and state observer used in this work given that the estimated state does not severely oscillate or blow up; i.e., the observer is well designed. Information about the time constant is valuable for gain scheduling when the observer is used to handle strong sensor noise.

The above analysis is based on a linearized version of the observer, and so the result is only an approximation. Nevertheless, this approximation is sufficiently good for practical applications, in particular gain scheduling, as shown in Section 4.4.

## 4 Results and Discussion

### 4.1 Model validation

Since the mechanistic model is a basis for state observer and control design, this section extensively validates the proposed model with three different datasets from the literature to ensure that our model provides an accurate prediction of the bound water concentration and product temperature.

The first dataset is obtained from the experimental data presented in [15], where the time profile of the total mass of residual water (bound water) during secondary drying was reported. Our mechanistic model can accurately predict the concentration of bound water, with the maximum error is about 0.01 kg water/kg solid (Fig. 3A). The concentration decreases exponentially following the linear driving force model.

The second dataset for model validation is the simulation result obtained from the high-fidelity model proposed by [16]; the model simulates simultaneous heat and mass transfer in 2D. Our model prediction agrees well the result obtained from the high-fidelity model (Fig. 3B), indicating that our simplified model, which simulates the system in 1D and omits mass transfer equations, can still accurately predict the time evolution of the bound water concentration, agreeing with the observation by [33].

The final dataset is obtained from [18], where the time profiles of both residual water and product temperature were reported. Our model can precisely simulate the product temperature (Fig. 3c). The model can also reasonably predict the concentration of bound water despite high uncertainty in the reported measurement.

The above three case studies show that our proposed model provides accurate prediction of the bound water concentration and product temperature during secondary drying, in comparison to experimental data and a model with higher fidelity.

### 4.2 Simulation-based observer design

This section focuses on the simulation-based observer design, with the default parameter values (see all parameter values in Supplementary Information). Practical observer design can be performed by running a series of simulations with different values of observer gains to understand the dynamics of the observer and find gain values that give satisfactory performance. Firstly, consider the observer gain  $L_T$ , which is directly related to the product temperature (Fig. 4A). The estimated average product temperature converges to the true value within 1 h for  $L_T = -1 \times 10^{-6}$  without any oscillation, which is relatively fast given the time scale of 12 h. Some oscillation is observed for  $L_T$  increased to  $5 \times 10^{-5}$ . The system is highly unstable and the estimated temperature blows up for  $L_T = 1 \times 10^{-4}$ , indicating

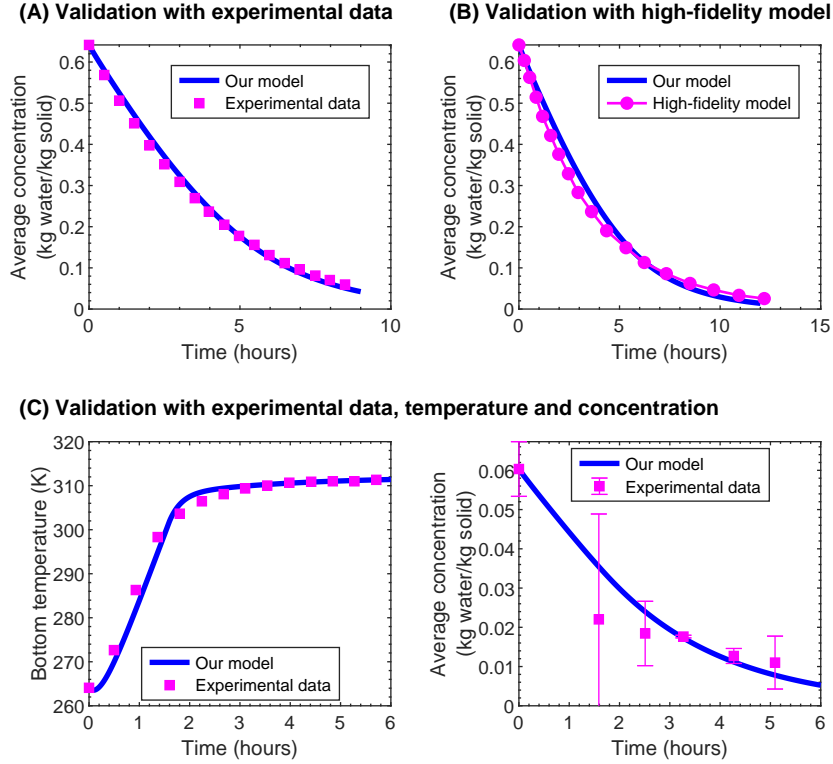


**Figure 3:** (A) Comparison between the concentration of bound water predicted by our model and the experimental data obtained from [15]. The original data reported as the total mass of water are normalized by the total mass of solid. The values of  $E_a$  and  $A$  estimated from data are  $5,000 \text{ J/mol}$  and  $7.1 \times 10^{-4} \text{ s}^{-1}$ , respectively. The initial concentration of bound water is  $0.6415 \text{ kg water/kg solid}$ . (B) Comparison between the concentration of bound water predicted by our model and the high-fidelity model by [16]. The original data reported as the total mass of water are normalized by the total mass of solid. The values of  $E_a$  and  $A$  estimated from data are  $5,000 \text{ J/mol}$  and  $7.1 \times 10^{-4} \text{ s}^{-1}$ , respectively. The initial concentration of bound water is  $0.6415 \text{ kg water/kg solid}$ . (C) Comparison between our model prediction and the experimental data from [18] for both temperature and concentration, with the reported  $E_a$  of  $5,920 \text{ J/mol}$ . The values of  $h$  and  $A$  estimated from data are  $9 \text{ W/(m}^2 \cdot \text{K)}$  and  $1.2 \times 10^{-3} \text{ s}^{-1}$ , respectively. Operating conditions were not reported, so the following are approximated from the data. The product and shelf temperatures are initially at  $264.09 \text{ K}$ . The shelf temperature increases at the rate of  $0.65 \text{ K/min}$ . The initial concentration of bound water is  $0.0603 \text{ kg water/kg solid}$ . Other parameters are kept at the default values.

that this observer gain is too high and suggesting that the sign of  $L_T$  is incorrect. Physically, when the estimated temperature is higher than the actual value, the observer term  $\mathbf{L}_T(\hat{\mathbf{T}} - \mathbf{T})$  should provide negative feedback to the observer to reduce the temperature, so  $L_T$  should be negative, agreeing with the result from Fig. 4A. With all the analysis in this part,  $L_T$  is set to  $-1 \times 10^{-6}$ .

Next, consider the observer gain  $L_c$  (Fig. 4B). This gain is more crucial than  $L_T$  as it is associated with the concentration of bound water, the most important state to be monitored during secondary drying. The estimated concentration blows up for  $L_c = -1 \times 10^{-7}$ , suggesting that the sign of  $L_c$  is wrong. This behavior is undesirable as it gives unrealistic process values, which could lead to errors or failure in related systems, e.g., control systems. With the positive observer gain  $L_c = 1 \times 10^{-8}$ , convergence can be observed. However, it takes more than 8 h to achieve the convergence, meaning that the observer reports an incorrect estimated state for most of the process operation. An observer with this sluggish convergence therefore is not beneficial. With a proper gain value,  $L_c = 5 \times 10^{-7}$ , the estimated concentration converges to the correct value without any oscillation in less than 2 h, which is fast compared to the time scale of 12 h. A slightly slower convergence is observed for the high case, which is reasonable as the initial estimated state is farther from the correct value. When the estimated temperature is higher than the actual value, it physically implies that the estimated desorption rate is too low. Therefore, the observer term  $\mathbf{L}_c(\hat{\mathbf{T}} - \mathbf{T})$  should provide positive feedback to the observer to increase the estimated concentration, and  $L_c$  should be positive. Based on this analysis, the observer gain  $L_c$  is set to  $5 \times 10^{-7}$ .

In Figs. 4AB, the convergence is demonstrated via the average properties as it is intuitive and easy to visualize, although the mechanistic model and state observer also estimate the spatial variation of those

properties. In Fig. 4C, the spatiotemporal evolution of the estimation errors is shown for both product temperature and bound water concentration, for  $L_T = -1 \times 10^{-6}$  and  $L_c = 5 \times 10^{-7}$ . The estimation errors decrease to zero in less than 2 h, showing that the observer can accurately estimate the spatial temperature and concentration, in addition to the average values.

Of course, there are other values for  $L_T$  and  $L_c$  that can give satisfactory performance. To provide a systematic study of the choice of observer gains, Fig. 4D plots the convergence times\* for different pairs of  $L_T$  and  $L_c$ ; this plot defines a design space for  $L_T$  and  $L_c$  where convergence can be achieved. The plot also highlights the fact that, although the estimation of the concentration is most important, both  $L_c$  and  $L_T$  need to be chosen well due to coupling between the species concentration and temperature equations, and a poor choice of value for  $L_T$  can result in slow convergence. In the later sections of this work,  $L_T = -1 \times 10^{-6}$  and  $L_c = 5 \times 10^{-7}$  are used as the default observer gains. This exact same analysis and design procedure can be used for the modified observer, with the final observer gains selected to be  $L_T = -5 \times 10^{-3}$  and  $L_c = 1 \times 10^{-4}$ .

Another important aspect of the observer is initialization. For the estimated temperature, it is logical to set the initial condition to be equal to the measured temperature. In Fig. 4, the initial estimated temperature is set to be higher than the measured value by 10% to demonstrate the convergence. The initial estimated concentration is, however, unknown as due to no real-time concentration measurement. In Fig. 4, we initialize the observer with the maximum and minimum concentrations (0.6415 kg water/kg solid and 0.0314 kg water/kg solid) reported in the literature [15, 41] to demonstrate the convergence under the worst-case scenarios. In practice, the initial estimated concentration could be set to some more realistic value specific to that system or experiment. This information should be obtained during the design and development phase, which could result in faster convergence. In the later sections of this work, the initial estimated concentration is set to 0.0314 kg water/kg solid and the initial estimated temperature is set to the measured value unless otherwise specified so that the observer performance is analyzed on the same basis.

### 4.3 Observer performance under various conditions

In the previous section, the observer is designed using the default parameter values. This section explores the performance of the designed observer under various conditions.

From the mechanistic understanding of desorption described in Section 2, three key parameters that directly influence the desorption dynamics are the frequency factor  $A$ , activation energy  $E_a$ , and concentration  $c_s$ . Hence, we study the performance of the observer for several values of  $A$ ,  $E_a$ , and  $c_{s,0}$  reported in the lyophilization literature.

The first part of the study focuses on the frequency factor  $A$ . The estimated state smoothly converges to the true state within 2 h from the time scale of 10 h for the low case (Fig. 5A1). An increase in the frequency factor reduces the time required for secondary drying to less than 8 h, in which the estimated state can converge to the true state within about 90 min (Fig. 5A2). Convergence is achieved for both spatial and average concentration.

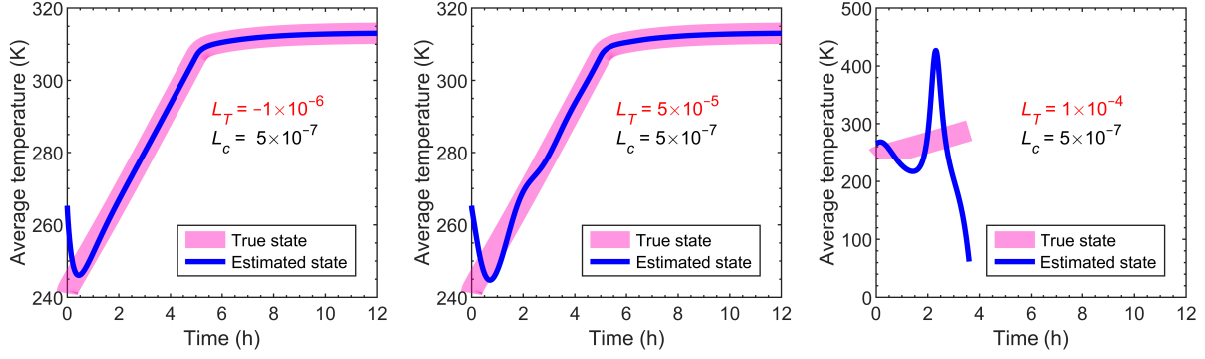
The second part of this analysis centers on the activation energy  $E_a$ . For the low case, the estimated concentration converges to the true value within 1 h from the time scale of about 4 h (Fig. 5B1). The dynamics of the process are relatively fast here compared to other cases, but the observer can still perform very well. For the high case, the convergence is observed at about 6 h from the time scale of about 45 h (Fig. 5B2). The drying time of 45 h is considered extremely slow for secondary drying, but that does not impact the performance of the observer.

The final part of this analysis considers the concentration level  $c_{s,0}$ . Regarding the low case, the initial estimated concentration is somehow correct, i.e., equal to the true value, so the convergence is

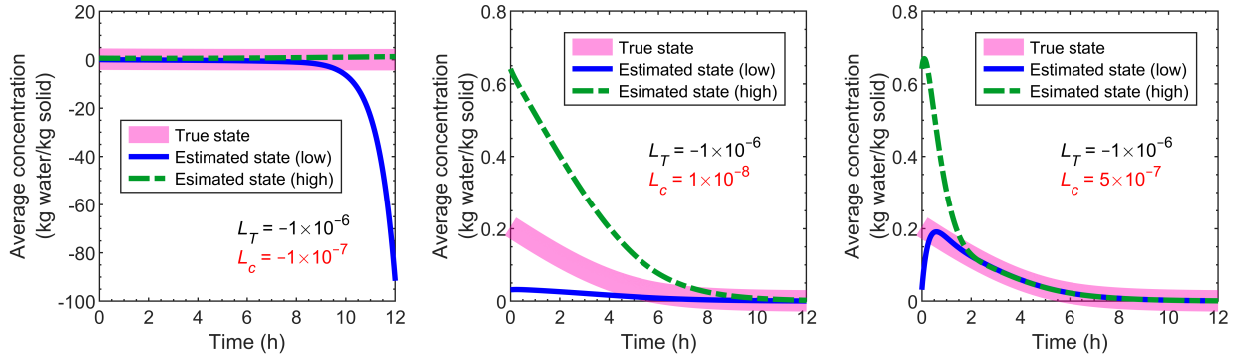
---

\*The convergence time is defined as the time required for the estimation error for concentration is less than 2% of its initial error.

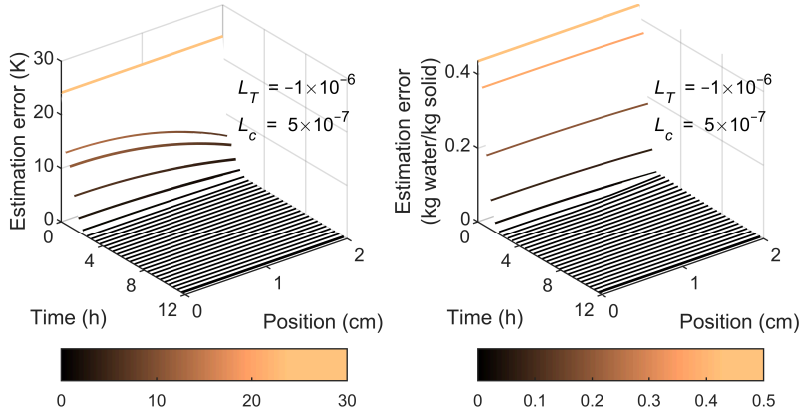
### (A) Observer gain selection for temperature



### (B) Observer gain selection for concentration



### (C) Spatiotemporal estimation errors for temperature and concentration



### (D) Design space for $L_T$ and $L_c$

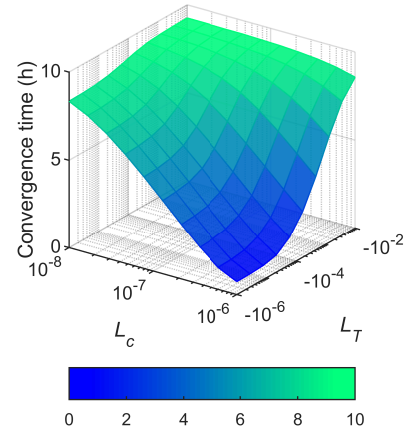


**Figure 4:** (A) Convergence of the estimated average product temperature for three different values of  $L_T$  while  $L_c$  is kept constant. The initial estimated temperature is set to be higher than the actual value by about 10% to demonstrate convergence. The initial concentration is treated as being known in this plot. (B) Convergence of the estimated average concentration of bound water at three different values of  $L_c$  while  $L_T$  is kept constant. The initial estimated concentration is set to the maximum (high) and minimum (low) realistic values reported in the literature, which are about 0.6145 kg water/kg solid and 0.0314 kg water/kg solid, respectively [15, 41]. The initial estimated temperature is set to be higher than the actual value by about 10%. (C) Spatiotemporal evolution of the estimation errors for both temperature and concentration (high) to indicate the convergence at all locations with the selected gains. d, Design space showing the times required for the estimated concentration to converge to the true value at different pairs of the observer gains  $L_T$  and  $L_c$ . Values of  $L_T$  and  $L_c$  outside this design space could lead to severe oscillation or divergence. All simulations are based on the default parameter values.

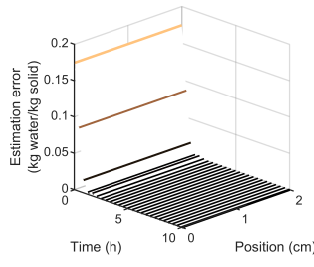
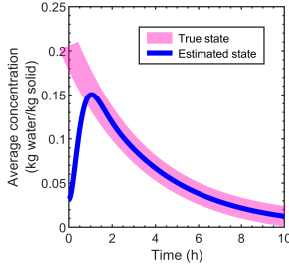
immediate (Fig. 5C1). For the high case, the convergence is observed at about 2 h from the time scale of 10 h (Fig. 5C2). The observer can converge quickly even when the initial estimated state is off by more than an order of magnitude; i.e., the initial estimated concentration is 0.0314 kg water/kg solid, whereas the true value is 0.6415 kg water/kg solid.

Results from this study show that the observer is able efficiently and accurately estimate the concentration of bound water for various desorption dynamics considered in the literature. The convergence

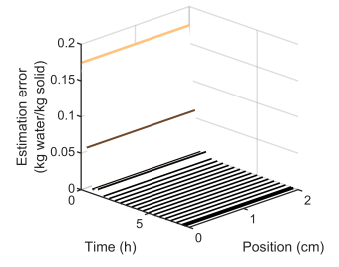
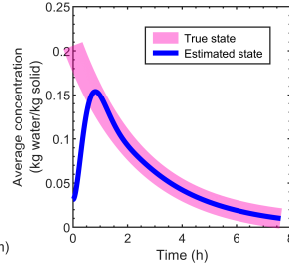
is achieved for every case study via a single observer design where  $L_T = -1 \times 10^{-6}$  and  $L_c = 5 \times 10^{-7}$ , indicating that the proposed observer and design strategy are robust.

### (A) Variation in frequency factor

#### 1. Low case, $A = 7.8 \times 10^{-5} \text{ s}^{-1}$

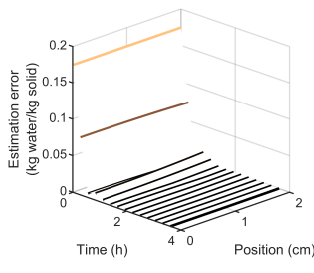
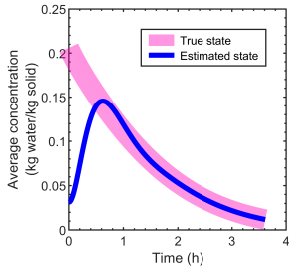


#### 2. High case, $A = 1.1 \times 10^{-4} \text{ s}^{-1}$

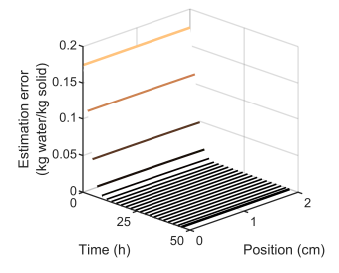
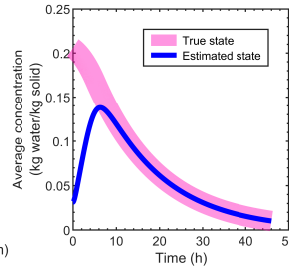


### (B) Variation in activation energy

#### 1. Low case, $E_a = 5,920 \text{ J/mol}$

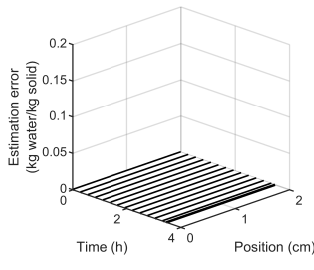
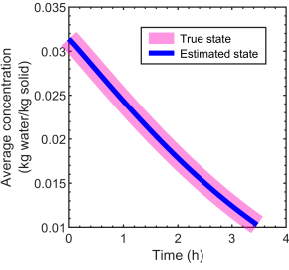


#### 2. High case, $E_a = 13,146 \text{ J/mol}$



### (C) Variation in initial concentration

#### 1. Low case, $c_{s,0} = 0.0314 \text{ kg water/kg solid}$



#### 2. High case, $c_{s,0} = 0.6415 \text{ kg water/kg solid}$

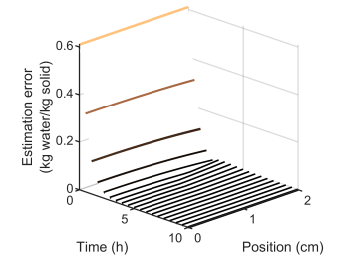
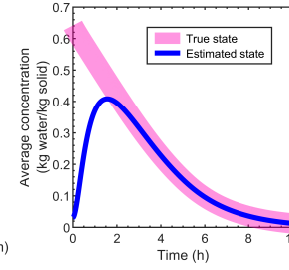


**Figure 5:** (A) Convergence of the estimated concentration for different frequency factors  $A$ . The frequency factor is varied between  $7.8 \times 10^{-5} \text{ s}^{-1}$  [16] and  $1.1 \times 10^{-4} \text{ s}^{-1}$  [14] given that the rate constant is independent on temperature. (B) Convergence of the estimated concentration for different activation energies  $E_a$ . The activation energy is varied between 5,920 J/mol [18] and 13,146 J/mol [42]. (C) Convergence of the estimated concentration for different initial concentrations,  $c_{s,0}$ . The initial condition is varied between 0.0314 kg water/kg solid [4] and 0.6415 kg water/kg solid [15]. In all cases, the simulations are terminated when the estimated concentration drops below 0.01 kg water/kg solid. The default observer gains  $L_T = -1 \times 10^{-6}$  and  $L_c = 5 \times 10^{-7}$  are used. Other parameters are kept at the default values.

## 4.4 Measurement noise and observer gain scheduling

A state observer always receives some form of measurement, and thus it is important to ensure that the estimated states are insensitive to measurement noise. A high observer gain could give fast convergence but also magnify the noise, resulting in inaccurate estimation of the states. This section discusses effects of measurement noise and demonstrates the corresponding observer design.

Using the default parameter values, independent normally distributed noise of standard deviation given by  $3\sigma = 5^\circ\text{C}$  is added to the temperature measurement [40]. The estimated concentration is severely polluted by the measurement noise for the default observer gain  $L_c = 5 \times 10^{-7}$  (Fig. 6A). Significant oscillation is observed, in which the observer does not give valuable information when the concentration is small (i.e., after about 6 h). To reduce the noise effect, the observer gain  $L_c$  is reduced to  $2 \times 10^{-7}$ . In comparison to  $L_c = 5 \times 10^{-7}$ , the convergence is achieved slightly slower, but the oscillation is much weaker. Reducing the gain  $L_c$  further to  $1 \times 10^{-7}$  almost removes the oscillation, but the convergence



is also significantly slower.

The above information motivates the use of observer gain scheduling, which is a technique that varies the observer gains with time to ensure satisfactory performance at different operating points, especially for nonlinear systems. In this case, we can initialize the observer with a high gain to achieve fast convergence, and then gradually switch to a low gain after some time to reduce oscillation. Here the switching time is set to  $t = 4\tau$ , where  $\tau$  is the time constant derived in Section 3.3. From the definition of the time constant,  $t = 4\tau$  should be the time when the estimation error is about 98% of the initial value, that is, when the estimated state has nearly converged to the true value. This technique enables fast convergence while having low effects of measurement noise on the state estimate (Fig. 6B).

This analysis highlights another benefit of the proposed observer in terms of noise filtering. Selecting the observer gain needs to trade off sensitivity to measurement noise with speed of convergence of the state estimates as demonstrated above. For this process, it is acceptable to allow for some small oscillation when the concentration is high (e.g., larger than 0.1) as the value is not affected much. However, oscillation should be minimized when the concentration is low, so that the final concentration of bound water can be accurately estimated to ensure product quality.

Note that the above noise level (Fig. 6C) is significantly higher than in actual experiments [40], and so the resulting design has a large safety margin to span the range of noise levels encountered in real temperature sensors. A lower safety margin, with faster convergence to the states, could be achieved by performing the analysis for a noise level set by experimental data for the specific temperature sensor used in the specific equipment.

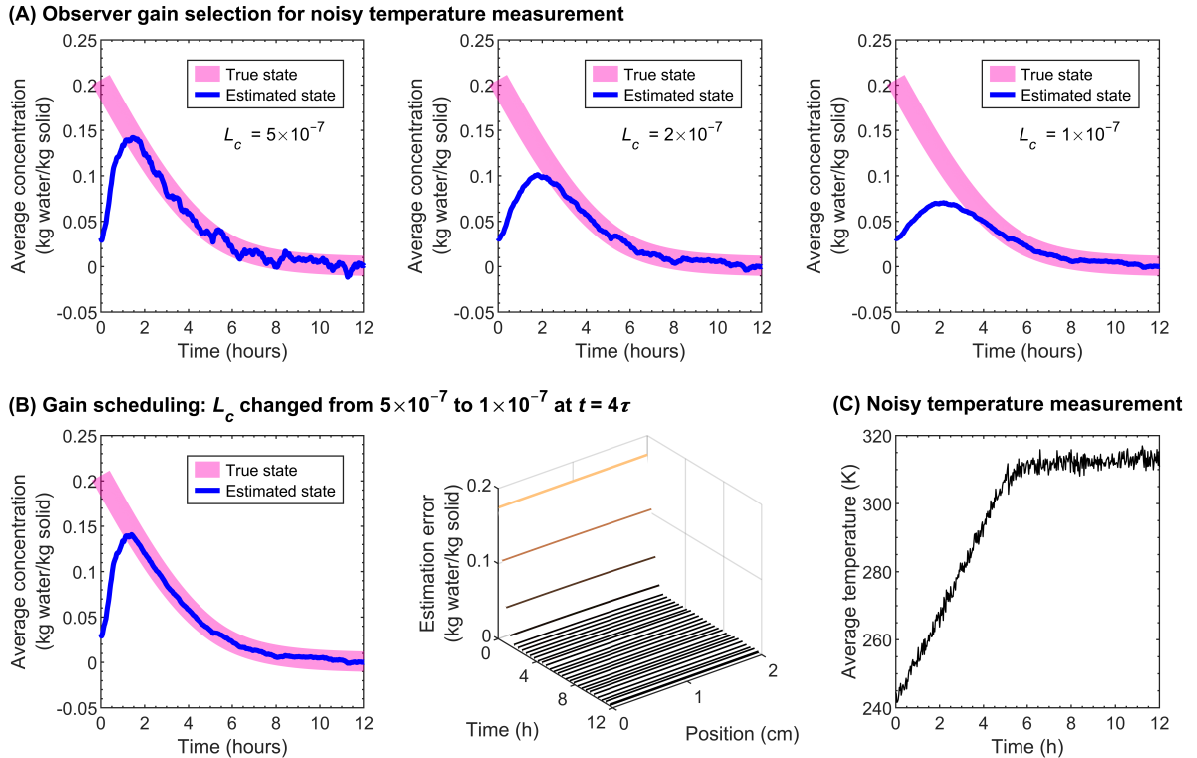


**Figure 6:** (A) Convergence and oscillation behavior of the estimated concentration at different observer gains  $L_c = 5 \times 10^{-7}$ ,  $2 \times 10^{-7}$ , and  $1 \times 10^{-7}$  while  $L_T$  is fixed at  $-1 \times 10^{-6}$  in all cases. (B) Gain scheduling technique where  $L_c$  is set to  $5 \times 10^{-7}$  for fast convergence at the beginning and then reduced to  $1 \times 10^{-7}$  at  $t = 4\tau$  to reduce the effect of measurement noise. (C) Noisy temperature data obtained from adding independent normally distributed noise of standard deviation given by  $3\sigma = 5^\circ\text{C}$  to the true state. Other parameters kept at their default values.



## 4.5 Experimental-based observer design

In the simulation-based observer design, the true and estimated states are simulated simultaneously and continuously. In real systems, measurement data are usually sampled and fed to a state observer in a discrete fashion, i.e., with a fixed sampling time. This section applies the proposed observer to estimate the concentration of bound water in four different experiments from the literature, denoted as Cases A [15], B [1], C [41], and D [4]. The temperature measurement is obtained and fed to the observer every 10 seconds. Parameter values and data preprocessing are described in Supplementary Information.

By using the default observer gains obtained from our simulation-based design, the observer can converge the estimated concentration to the correct value in less than 2 h for all four experiments, showing the robustness of our design (Fig. 7). In Figs. 7AB, two experiments with spatially distributed temperature measurement are considered, and so the state observer is used as usual. In Figs. 7CD, the only measurement available is the bottom temperature, and so the modified state observer is used instead (see Section 3.2). Both the original and modified observers work perfectly. The observer with spatially distributed measurement provides more complete information of the product. In addition, sensors, e.g., IR cameras, are always located outside a vial, enabling non-contact measurement. The observer with point measurement, e.g., a thermocouple, would lead to a more simple and less expensive setup, with lower noise and bias [43].

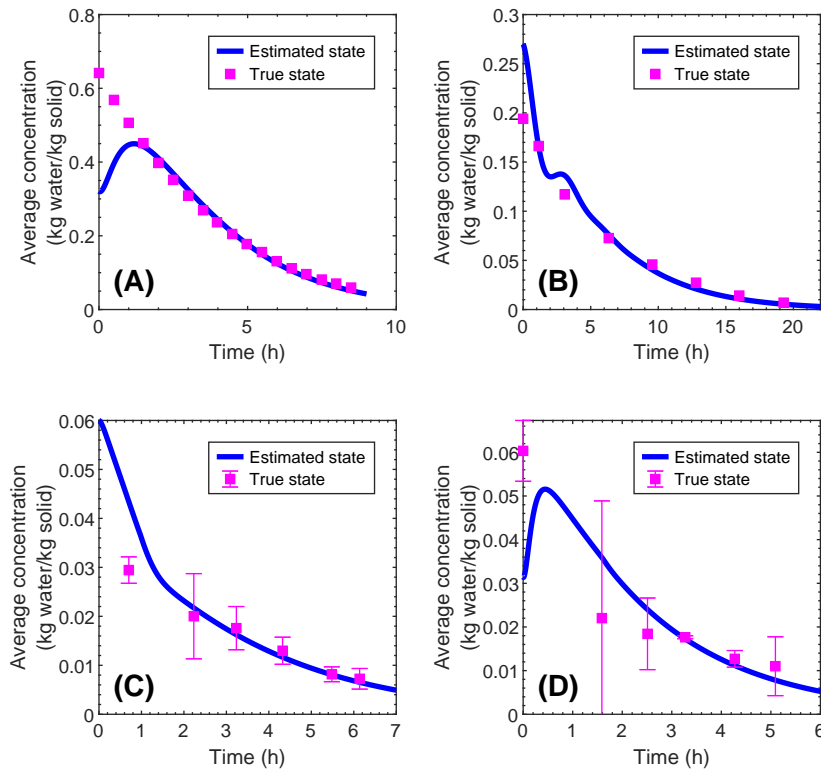


**Figure 7:** Convergence of the estimated concentration when applying the state observer to the real systems in Case A (Panel A) and Case B (Panel B). Convergence of the estimated concentration when applying the modified state observer to the real systems in Case C (Panel C) and Case D (Panel D). In all case studies, the sampling time of 10 seconds is used, with the default parameter values and observer gains. The initial estimated concentration is chosen to be lower/higher than the true value by about 20%–100% to demonstrate convergence. The initial estimated temperature is set to the measured value.

The choice of sampling time needs to be considered when implementing a state observer to the real system. If the sampling time is too large, the observer could converge slowly or diverge due to insufficient measurement information. Also, the sampling time must be higher than the computation time required for simulating the observer in each time step. Our observer can be simulated in less than a second on a normal laptop, and thus the sampling time of 10 seconds is more than adequate. The sampling time should also be chosen to be sufficiently small compared to the time scale of a process to ensure that any

important dynamics are well captured. For example, the time scale of 10 seconds is reasonable given the time scale of many hours in lyophilization.

The heat transfer dynamics predicted by the model is a function of the heat transfer coefficient  $h$ , which is estimated from data and so can have some uncertainty. For the experimental data from Cases A [15] and B [1], our observer converges the estimated states to the correct values even for 10% error in the value of the heat transfer coefficient (Fig. 8). The convergence is slightly slower, but the difference is nearly unnoticeable (cf., Figs. 7AB and 8AB). Our estimates of average concentration is insensitive to uncertainty in the heat transfer coefficient.

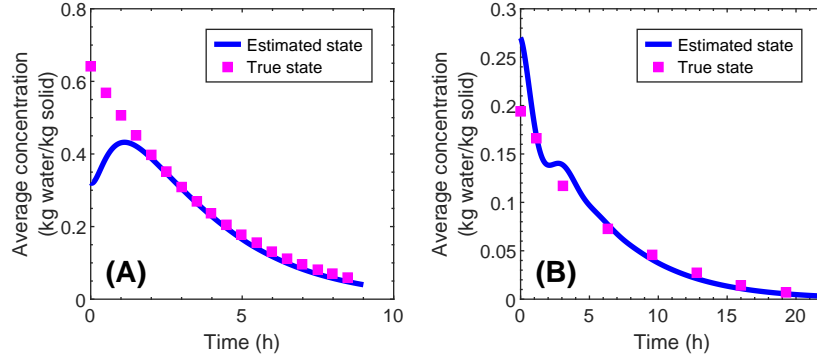


**Figure 8:** Convergence of the estimated concentration when applying the state observer Case A (Panel A) and Case B (Panel B). The value of the heat transfer coefficient  $h$  for the observer is set to be 10% lower than the correct value for Case A and 10% higher than the correct value for Case B. The sampling time of 10 seconds is used, with the default parameter values and observer gains. The initial estimated concentration is chosen to be different from the correct value to demonstrate convergence. The initial estimated temperature is set to the measured value.

## 5 Conclusion

This article describes a new approach for the real-time estimation of bound water concentration during desorption, with application to secondary drying in lyophilization. The technique relies on a state observer, in particular a Luenberger observer, which uses the information from mechanistic understanding of the process and temperature measurement to predict the concentration of bound water. Our observer can accurately estimate the concentration for various desorption dynamics, noisy data, and real experiments. Nearly all the case studies presented in this work, except for the noise and fine-tuning parts, are achieved by a single observer design, indicating high robustness of the observer.

The proposed framework is designed to be simple and practical for implementation. The observer can be simulated in real-time, with the computation time of less than a second on a normal laptop. No concentration measurement is required; only temperature measurement is necessary. As temperature measurement is straightforward and commonly required in every step of lyophilization, the technique can be employed with a very simple setup and operation compared to any other methods. The approach is presented systematically, with detailed derivation and mathematical analysis, and so it can be easily extended to desorption-based processes other than lyophilization. This extension can be done by rewriting a mechanistic model for the new system and redesigning a state observer using the procedure described in this article.

## **Data Availability**

All software and data will be made available upon publication of the manuscript.

## **Acknowledgements**

This research was supported by the U.S. Food and Drug Administration under the FDA BAA-22-00123 program, Award Number 75F40122C00200.

## References

- [1] A. Liapis, R. Bruttini, A theory for the primary and secondary drying stages of the freeze-drying of pharmaceutical crystalline and amorphous solutes: Comparison between experimental data and theory, *Separations Technology* 4 (3) (1994) 144–155. doi:10.1016/0956-9618(94)80017-0.
- [2] H. Muramatsu, K. Lam, C. Bajusz, D. Laczko, K. Karikó, P. Schreiner, A. Martin, P. Lutwyche, J. Heyes, N. Pardi, Lyophilization provides long-term stability for a lipid nanoparticle-formulated, nucleoside-modified mRNA vaccine, *Molecular Therapy* 30 (5) (2022) 1941–1951. doi:10.1016/j.ymthe.2022.02.001.
- [3] S. Meulewaeter, G. NuFyten, M. H. Cheng, S. C. De Smedt, P. R. Cullis, T. De Beer, I. Lentacker, R. Verbeke, Continuous freeze-drying of messenger RNA lipid nanoparticles enables storage at higher temperatures, *Journal of Controlled Release* 357 (2023) 149–160. doi:10.1016/j.jconrel.2023.03.039.
- [4] D. Fissore, R. Pisano, A. A. Barresi, Process analytical technology for monitoring pharmaceuticals freeze-drying – A comprehensive review, *Drying Technology* 36 (15) (2018) 1839–1865. doi:10.1080/07373937.2018.1440590.
- [5] R. Pisano, D. Fissore, S. A. Velardi, A. A. Barresi, In-line optimization and control of an industrial freeze-drying process for pharmaceuticals, *Journal of Pharmaceutical Science* 99 (11) (2010) 4691–4709. doi:10.1002/jps.22166.
- [6] S. A. Velardi, A. A. Barresi, Development of simplified models for the freeze-drying process and investigation of the optimal operating conditions, *Chemical Engineering Research and Design* 86 (1) (2008) 9–22. doi:10.1016/j.cherd.2007.10.007.
- [7] J. H. Gitter, R. Geidobler, I. Presser, G. Winter, Microwave-assisted freeze-drying of monoclonal antibodies: Product quality aspects and storage stability, *Pharmaceutics* 11 (12) (2019) 674. doi:10.3390/pharmaceutics11120674.
- [8] M. J. Pikal, W. J. Mascarenhas, H. U. Akay, S. Cardon, C. Bhugra, F. Jameel, S. Rambhatla, The nonsteady state modeling of freeze drying: In-process product temperature and moisture content mapping and pharmaceutical product quality applications, *Pharmaceutical Development and Technology* 10 (1) (2005) 17–32. doi:10.1081/PDT-35869.
- [9] D. Fissore, R. Pisano, A. A. Barresi, Monitoring of the secondary drying in freeze-drying of pharmaceuticals, *Journal of Pharmaceutical Sciences* 100 (2) (2011) 732–742. doi:10.1002/jps.22311.
- [10] C. Ikeda, G. Zhou, Y.-C. Lee, G. Chouzouri, L. Howell, B. Marshall, L. Bras, Application of online NIR spectroscopy to enhance process understanding and enable in-process control testing of secondary drying process for a spray-dried solid dispersion intermediate, *Journal of Pharmaceutical Sciences* 111 (9) (2022) 2540–2551. doi:10.1016/j.xphs.2022.04.009.
- [11] S. C. Schneid, H. Gieseler, W. J. Kessler, S. A. Luthra, M. J. Pikal, Optimization of the secondary drying step in freeze drying using TDLAS technology, *AAPS PharmSciTech* 12 (1) (2011) 379–387. doi:10.1208/s12249-011-9600-7.
- [12] D. Luenberger, An introduction to observers, *IEEE Transactions on Automatic Control* 16 (6) (1971) 596–602. doi:10.1109/TAC.1971.1099826.
- [13] R. Litchfield, A. Liapis, An adsorption-sublimation model for a freeze dryer, *Chemical Engineering Science* 34 (9) (1979) 1085–1090. doi:10.1016/0009-2509(79)85013-7.
- [14] W. Mascarenhas, H. Akay, M. Pikal, A computational model for finite element analysis of the freeze-drying process, *Computer Methods in Applied Mechanics and Engineering* 148 (1) (1997) 105–124. doi:10.1016/S0045-7825(96)00078-3.

- [15] H. Sadikoglu, A. I. Liapis, Mathematical modelling of the primary and secondary drying stages of bulk solution freeze-drying in trays: Parameter estimation and model discrimination by comparison of theoretical results with experimental data, *Drying Technology* 15 (3-4) (1997) 791–810. doi:[10.1080/07373939708917262](https://doi.org/10.1080/07373939708917262).
- [16] P. Sheehan, A. I. Liapis, Modeling of the primary and secondary drying stages of the freeze drying of pharmaceutical products in vials: Numerical results obtained from the solution of a dynamic and spatially multi-dimensional lyophilization model for different operational policies, *Biotechnology and Bioengineering* 60 (6) (1998) 712–728. doi:[10.1002/\(SICI\)1097-0290\(19981220\)60:6<712::AID-BIT8>3.0.CO;2-4](https://doi.org/10.1002/(SICI)1097-0290(19981220)60:6<712::AID-BIT8>3.0.CO;2-4).
- [17] J. Nastaj, K. Witkiewicz, Mathematical modeling of the primary and secondary vacuum freeze drying of random solids at microwave heating, *International Journal of Heat and Mass Transfer* 52 (21) (2009) 4796–4806. doi:[10.1016/j.ijheatmasstransfer.2009.06.015](https://doi.org/10.1016/j.ijheatmasstransfer.2009.06.015).
- [18] D. Fissore, R. Pisano, A. A. Barresi, Using mathematical modeling and prior knowledge for QbD in freeze-drying processes, in: F. Jameel, S. Hershenson, M. A. Khan, S. Martin-Moe (Eds.), *Quality by Design for Biopharmaceutical Drug Product Development*, Springer, New York, 2015, pp. 565–593. doi:[10.1007/978-1-4939-2316-8\\_23](https://doi.org/10.1007/978-1-4939-2316-8_23).
- [19] J. Mohd Ali, N. Ha Hoang, M. A. Hussain, D. Dochain, Review and classification of recent observers applied in chemical process systems, *Computers & Chemical Engineering* 76 (2015) 27–41. doi:[10.1016/j.compchemeng.2015.01.019](https://doi.org/10.1016/j.compchemeng.2015.01.019).
- [20] S. A. Velardi, H. Hammouri, A. A. Barresi, In-line monitoring of the primary drying phase of the freeze-drying process in vial by means of a Kalman filter based observer, *Chemical Engineering Research and Design* 87 (10) (2009) 1409–1419. doi:[10.1016/j.cherd.2009.03.011](https://doi.org/10.1016/j.cherd.2009.03.011).
- [21] H. H. Salvatore A. Velardi, A. A. Barresi, Development of a high gain observer for in-line monitoring of sublimation in vial freeze drying, *Drying Technology* 28 (2) (2010) 256–268. doi:[10.1080/07373930903530204](https://doi.org/10.1080/07373930903530204).
- [22] S. Bosca, D. Fissore, Design and validation of an innovative soft-sensor for pharmaceuticals freeze-drying monitoring, *Chemical Engineering Science* 66 (21) (2011) 5127–5136. doi:[10.1016/j.ces.2011.07.008](https://doi.org/10.1016/j.ces.2011.07.008).
- [23] S. Bosca, A. A. Barresi, D. Fissore, Use of a soft sensor for the fast estimation of dried cake resistance during a freeze-drying cycle, *International Journal of Pharmaceutics* 451 (1) (2013) 23–33. doi:[10.1016/j.ijpharm.2013.04.046](https://doi.org/10.1016/j.ijpharm.2013.04.046).
- [24] E. N. Drăgoi, S. Curteanu, D. Fissore, On the use of artificial neural networks to monitor a pharmaceutical freeze-drying process, *Drying Technology* 31 (1) (2013) 72–81. doi:[10.1080/07373937.2012.718308](https://doi.org/10.1080/07373937.2012.718308).
- [25] S. Bosca, A. A. Barresi, D. Fissore, Design of a robust soft-sensor to monitor in-line a freeze-drying process, *Drying Technology* 33 (9) (2015) 1039–1050. doi:[10.1080/07373937.2014.982250](https://doi.org/10.1080/07373937.2014.982250).
- [26] S. Bosca, A. A. Barresi, D. Fissore, On the robustness of the soft sensors used to monitor a vial freeze-drying process, *Drying Technology* 35 (9) (2017) 1085–1097. doi:[10.1080/07373937.2016.1243553](https://doi.org/10.1080/07373937.2016.1243553).
- [27] D. Fissore, R. Pisano, A. A. Barresi, On the use of temperature measurement to monitor a freeze-drying process for pharmaceuticals, in: *IEEE International Instrumentation and Measurement Technology Conference*, 2017, pp. 1–6. doi:[10.1109/I2MTC.2017.7969890](https://doi.org/10.1109/I2MTC.2017.7969890).
- [28] S. Bosca, A. Barresi, D. Fissore, On the use of model-based tools to optimize in-line a pharmaceuticals freeze-drying process, *Drying Technology* 34 (15) (2016) 1831–1842. doi:[10.1080/07373937.2016.1146755](https://doi.org/10.1080/07373937.2016.1146755).

- [29] D. Fissore, S. A. Velardi, A. A. Barresi, In-line control of a freeze-drying process in vials, *Drying Technology* 26 (6) (2008) 685–694. doi:10.1080/07373930802046161.
- [30] A. A. Barresi, S. A. Velardi, R. Pisano, V. Rasetto, A. Vallan, M. Galan, In-line control of the lyophilization process. A gentle PAT approach using software sensors, *International Journal of Refrigeration* 32 (5) (2009) 1003–1014. doi:10.1016/j.ijrefrig.2008.10.012.
- [31] M. U. H. Joardder, M. Mourshed, M. Hasan Masud, *Bound Water Measurement Techniques*, Springer International Publishing, Cham, 2019, pp. 47–82. doi:10.1007/978-3-319-99888-6\_4.
- [32] M. Harguindeguy, L. Stratta, D. Fissore, R. Pisano, Combining mathematical modeling and thermal infrared data in the freezing of pharmaceutical liquid formulations, *Industrial & Engineering Chemistry Research* 61 (12) (2022) 4379–4389. doi:10.1021/acs.iecr.1c04595.
- [33] K. Yoon, V. Narsimhan, Understanding heat transfer during the secondary drying stage of freeze drying: Current practice and knowledge gaps, *Journal of Pharmaceutical Sciences* 111 (2) (2022) 368–381. doi:10.1016/j.xphs.2021.09.032.
- [34] M. Fayaz, P. Shariaty, J. D. Atkinson, Z. Hashisho, J. H. Phillips, J. E. Anderson, M. Nichols, Using microwave heating to improve the desorption efficiency of high molecular weight VOC from beaded activated carbon, *Environmental Science & Technology* 49 (7) (2015) 4536–4542. doi:10.1021/es505953c.
- [35] A. Abdelraheem, R. Tukra, P. Kazarin, M. D. Sinanis, E. M. Topp, A. Alexeenko, D. Peroulis, Statistical electromagnetics for industrial pharmaceutical lyophilization, *PNAS Nexus* 1 (3) (2022) pgac052. doi:10.1093/pnasnexus/pgac052.
- [36] W. Wang, S. Zhang, Y. Pan, J. Yang, Y. Tang, G. Chen, Multiphysics modeling for microwave freeze-drying of initially porous frozen material assisted by wave-absorptive medium, *Industrial & Engineering Chemistry Research* 59 (47) (2020) 20903–20915. doi:10.1021/acs.iecr.0c03852.
- [37] S. Sircar, J. R. Hufton, Why does the linear driving force model for adsorption kinetics work?, *Adsorption* 6 (2000) 137–147. doi:10.1023/A:1008965317983.
- [38] E. K. Sahni, M. J. Pikal, Modeling the secondary drying stage of freeze drying: Development and validation of an excel-based model, *Journal of Pharmaceutical Sciences* 106 (3) (2017) 779–791. doi:10.1016/j.xphs.2016.10.024.
- [39] W. Schiesser, *The Numerical Method of Lines: Integration of Partial Differential Equations*, Academic Press, San Diego, 1991.
- [40] P. Srisuma, A. Pandit, Q. Zhang, M. S. Hong, J. Gamekkanda, F. Fachin, N. Moore, D. Djordjevic, M. Schwaerzler, T. Oyetunde, W. Tang, A. S. Myerson, G. Barbastathis, R. D. Braatz, Thermal imaging-based state estimation of a Stefan problem with application to cell thawing, *Computers & Chemical Engineering* 173 (2023) 108179. doi:10.1016/j.compchemeng.2023.108179.
- [41] R. Pisano, D. Fissore, A. A. Barresi, Quality by design in the secondary drying step of a freeze-drying process, *Drying Technology* 30 (11-12) (2012) 1307–1316. doi:10.1080/07373937.2012.704466.
- [42] I. Oddone, A. A. Barresi, R. Pisano, Influence of controlled ice nucleation on the freeze-drying of pharmaceutical products: The secondary drying step, *International Journal of Pharmaceutics* 524 (1) (2017) 134–140. doi:10.1016/j.ijpharm.2017.03.077.
- [43] E. Lietta, D. Colucci, G. Distefano, D. Fissore, On the use of IR thermography for monitoring a vial freeze-drying process, *Journal of Pharmaceutical Sciences* 108 (2019) 391–398. doi:10.1016/j.xphs.2018.07.025.